Journal of Mines, Metals and Fuels, *71(11): 2268-2277; 2023. DOI: 10.18311/jmmf/2023/36049*

Print ISSN : 0022-2755

Journal of Mines, Metals and Fuels

Contents available at: *www.informaticsjournals.com/index.php/jmmf*

Three-Dimensional Boundary-Layer Flow Across a Wedge: A Numerical Investigation

S. Shashi Prabha Gogate* and M. M. Praveena

Department of Mathematics, M.S. Ramaiah Institute of Technology (Affiliated to VTU), Bengaluru -560054, India; shashi.jan5@gmail.com

Abstract

The present work investigates the flow of a continuous, laminar, 3-D boundary-layer over a fixed wedge, where the outside free-stream flows are approximately approximated by a power of distances. The controlling partial differential equations are transformed into coupled nonlinear ordinary differential equations with the necessary boundary conditions using surface similarity transformations. These equations involve two physical variables: pressure gradient and shear-to-strain rate. The resulting equations are numerically solved by the implicit finite-difference scheme known as the Keller-box approach. The obtained results are compared with those reported in the literature for a few special cases. Our numerical results indicate that the flow zone is divided into two areas: near-field (close to the wedge surface) and far-field field (mostly controlled by inviscid flow).

Keywords: *Boundary-layer, Keller-box, Numerical Simulation, Similar Solution, Three-dimensional*

1.0 Introduction

Due to the mathematical complexity, it is challenging to analyse a general 3-D boundary-layer flow in which the velocity components rely on all the space coordinates. Three-dimensional flows over a surface can be studied using advanced numerical techniques and logical mathematical analysis. Most applications, including those involving aircraft wings with leading edges that are not perpendicular to the wing, such as swept and yawed wings, often involve three flows. It is assumed that the effects of viscosity are limited to a thin layer adjacent to the surface of the body in the case of flow past a body of generic shape. In a three-dimensional example, the real main-stream flow is dependent on all three spatial coordinates, and any fluctuations in the pressure along the normal would be disregarded. Two space coordinates measured along the surface are all that are needed to determine the flow that is immediately outside the boundary layer, which is believed to be an inviscid flow. Two new special effects that were not present in two-dimensional flow are now present in three-dimensional flow. The first of these effects is brought on by the convergence or divergence of the main flow's parallel surface streamlines, and the second effect is brought on by the curvature of these streamlines. Only when the pressure varies in such a way that continuity necessitates convergence in a direction other than normal to the surface do three-dimensional effects appear (Rosenhead[1]).

Getting the equations for a motion for boundary-layer flow over the three-dimensional body is the goal of the current effort. Howarth[2] introduced the flow around a stagnation point on a generic surface, which serves as the primary source for the three-dimensional boundary layer equations. 3-D boundary-layers are dominated by the two major free-stream flows (inviscid flow), much as in the case of two-dimensional flow where there is only one mainstream flow. This leads to the same results

**Author for correspondence*

for boundary layer equations. Similar to the traditional two-dimensional flow, the velocity components of the mainline flow may then be controlled by power-law relations in both the and directions. Howarth[3] created numerical solutions to the boundary-layer equations for three-dimensional stagnation point flows and depicted the flow's nodal points of attachment. Weidman[4] found asymptotic solutions for the behaviour in the far field during recent work on non-axisymmetric stagnation point flow in three-dimensional boundary layers. The velocity profiles with sample similarity, displacement thickness, and range-varying wall shear stress features are included in the results. Howarth[5] provided the solution for a one-parameter family of non-axisymmetric stagnation-point flows consisting of two orthogonal Hiemenz flows, which denote the strain rates of the superposed Hiemenz flows. Howarth only provided solutions within the range ($0 \le \alpha \le 1$), but he indicated that by applying the proper transformations, solutions outside of this range might be achieved. Davey[6] claims that a weakness in Howarth's work prevented solutions for the region from being extrapolated from those found for ($0 \le \alpha \le 1$). After that, Davey[6] looked into these saddle-point solutions for Howarth's formulas. Afterwards, the dual solutions to Howarth's equations were reported by Davey[6], Libby[7], Schofield and Davey[8]. Only the velocity field was examined in Wang[9] examination of the constant three-dimensional flow caused by a stretching plate. The unstable three-dimensional flow brought on by a flat surface extending in two lateral directions was then included by Surma Devi *et al.*[10] as an extension of this issue. The continuum of states shown in Howarth's equations was fully explained by the research of Hewitt, Duck, and Stow[11].

We learned from the literature review that the research of three-dimensional boundary layers is limited to just stagnation point flow with a few exceptions. In the current paper, we will demonstrate 3-D boundary-layer fluid flow over a wedge surface using two mainstream flows that are roughly represented by a power of distance of the form $U_\infty x^m$ and $V_\infty y^m$, where U_∞, V_∞, and m are constants and x and y are mainstream flow directions. Bernoulli's law can always be used to link pressure gradient to mainstream flows because pressure variation is uniform throughout the flow field. Now, the pressure gradient's strength is defined by the constant m. When $m=0$, the flow is over a flat surface and is considered to have a favourable pressure gradient for $m>0$ and an adverse pressure gradient for $m<0$. The Prandtl's boundary-layer exhibits self-similar solutions through similarity transformations, and these power-law approximations greatly simplify it (see next section for derivation).

The structure of the essay is as follows. We provide the 3-D boundary-layer flow over a wedge surface problem formulations in *S2*. The governing equations have been converted into third order coupled ordinary differential equations using similarity transformations. These equations are nonlinear and cannot be resolved analytically. Therefore, they have been resolved using the numerical Keller-box approach, or implicit finite-difference methodology. The techniques employed have previously been applied to a number of challenging issues. Given in *S3* are the method's steps and the convergence criteria that apply to numerical solutions. Using the aforementioned method, we looked at how the pressure gradient and shear-to-strain rate are two parameters that affect how the flow is modified. Finally, we offer a wide range of important findings in *S4*.

2.0 Formulation

The wedge's surface and the z normal to it are measured along the x, y, and z, axes, respectively, in the physical configuration of the current inquiry. If a wedge is at rest and there is a continuous three-dimensional laminar boundary layer flow across it, the flow is in the half-space $z>0$. When a fluid with constant density and viscosity is forced across a surface, it is anticipated that viscosity effects will only affect the boundary surface and that flow further from the surface will be controlled by a potential flow. The Navier-Stokes equations regulate the flow. The continuity and momentum equations for an incompressible fluid's steady three-dimensional flow are

$$\nabla \cdot \vec{V} = 0 \tag{1}$$

$$(\vec{V} \cdot \nabla)\vec{V} = -\frac{1}{\rho}\nabla p + \frac{\mu}{\rho}\nabla^2 \vec{V} \tag{2}$$

where p is the pressure and $V(\in u, v, w)$ is the velocity vector in the x, y, and z, directions. Furthermore, for flows with high Reynolds numbers, the effects of viscosity are limited to a narrow layer close to the surface's edge. A very

significant velocity gradient, $\frac{\partial u}{\partial x}$, $\frac{\partial v}{\partial x}$, $\frac{\partial u}{\partial y}$, $\frac{\partial v}{\partial y}$, $\frac{\partial v}{\partial x}$, $\frac{\partial v}{\partial y}$, $\frac{\partial v}{\partial y}$, exists inside this thin layer. The continuity and momentum equations are respectively written as under standard boundary-layer approximations (Schlichting and Gersten[12]).

$$\frac{\partial u}{\partial x}+\frac{\partial v}{\partial y}+\frac{\partial w}{\partial z}=0, \tag{3}$$

$$u\frac{\partial u}{\partial x}+v\frac{\partial u}{\partial y}+w\frac{\partial u}{\partial z}=U\frac{dU}{dx}+\nu\frac{\partial^2 u}{\partial z^2}, \tag{4}$$

$$u\frac{\partial v}{\partial x}+v\frac{\partial v}{\partial y}+w\frac{\partial v}{\partial z}=V\frac{dV}{dy}+\nu\frac{\partial^2 v}{\partial z^2}, \tag{5}$$

$$0=\frac{\partial p}{\partial z}, \tag{6}$$

and the corresponding relevant boundary conditions are

$$at\ z=0: \quad u=v=w=0, \qquad and \tag{7}$$

$$as\ z\to\infty: \quad u\to U \qquad and \qquad v\to V \tag{8}$$

ν is the kinematic viscosity of the fluid and $U=U(x)$ and $V=V(y)$ are velocities in the x- and y- directions beyond the boundary layer region. Due to the boundary conditions (cf. eq. 7), both velocities vary from zero at the surface to the major flows at great distances. Enforcing these constraints will cause all similarity solutions to decay (approach) appropriately for the far-field condition; the accommodation of decaying solutions depends on the flow parameters. According to equation (6), there is no normal pressure gradient. Along the boundary, a power-law change in the coordinate distance is anticipated for both potential flow velocities.

$$U(x)=U_\infty x^m, \qquad V(y)=V_\infty y^m \tag{9}$$

where $U_\infty V_\infty$ and m are constants.The pressure gradient's strength is indicated by the variable m. The three unknown velocity components in (4 and 5) can be readily reduced by introducing two unknown stream functions Ψ_1 and Ψ_2 as the pressure is a known impressed quantity.

$$\psi_1=\left(\frac{2\nu xU}{m+1}\right)^{\frac{1}{2}}f(\eta),\ \psi_2=\left(\frac{2\nu y\alpha V}{m+1}\right)^{\frac{1}{2}}g(\eta)\ and\ \eta=\left(\frac{(m+1)U}{2\nu x}\right)^{\frac{1}{2}}z. \tag{10}$$

where $f(n)$ and $g(n)$ are stream functions that are not dimensional. The velocity components $u=\frac{\partial\psi_1}{\partial z}$, $v=\frac{\partial\psi_2}{\partial z}$, and $w=-\left(\frac{\partial\psi_1}{\partial x}+\frac{\partial\psi_2}{\partial y}\right)$ are then connected to these stream functions Ψ_1 and Ψ_2. Similarity transformations enable the reduction of the three independent variables to only one. We obtain a system of connected third order nonlinear ordinary differential equations using these changes.

$$f'''(\eta)+f''(\eta)(f(\eta)+\alpha\beta g(\eta))+\beta(1-f'^2(\eta))=0 \tag{11}$$

$$g'''(\eta)+g''(\eta)(f(\eta)+\alpha\beta g(\eta))+\alpha\beta(1-g'^2(\eta))=0 \tag{12}$$

with boundary conditions

$$f(\eta)=g(\eta)=f'(\eta)=g'(\eta)=0 \quad when \quad \eta=0$$

$$f'(\eta)\to 1, \quad g'(\eta)\to 1 \quad as \quad \eta\to\infty \tag{13}$$

where η is a similarity parameter, $\beta=\frac{2m}{m+1}$ is the pressure gradient parameter, and $\beta>0$ denotes a favourable pressure gradient and $\beta<0$ a negative pressure gradient. While $\alpha=\frac{V_x}{U_y}$ is the shear-to-strain-rate parameter and $\beta=0$ signifies the flow past a flat plate. In order to eliminate dependency on x and y in the final equations because the wedge surface is fairly large according to Benzi *et al.*[13,14], we replace x and y by L (L is the reference length of the surface). Therefore, $\alpha=U_\infty V_\infty$. Note that the aforementioned system simplifies to the stagnation point flow for $\beta=1$. (Rosenhead[1]). Also take note of the fact that the aforementioned equation is new to the literature. We arrive to several conclusions that have been discussed in the literature: When, the previously indicated system (11)–(12) is equivalent to the conventional two-dimensional Falkner-Skan flow for $\alpha=1$. The flow around a body of revolution symmetrically positioned in a stream is represented by the above system, (11–12). The Homann's flow system, where $g(\eta)=f(\eta)$ and $\beta=1$, is the previously discussed system.

Additionally, numerical calculations for various values of *alpha* were made in the current work while taking the effects of the pressure gradient into account. The

aforementioned system is unable to provide a solution for $\beta = 0$, in the two-dimensional situation (Falkner-Skan equation).

3.0 Solution Method

Nonlinear problems are notoriously challenging to solve and make up the majority of problems in science and engineering. Boundary layer equations in three dimensions are essentially coupled systems with physical parameters. The linked system is always made more complex by nonlinearity and infinite interval. Only weakly nonlinear or linear problems can be approximated analytically using traditional methods, whereas strong nonlinear problems frequently fail to do so. Therefore, one must create reliable and precise numerical procedures for their solutions. In order to solve the whole nonlinear system, one can use the Keller-box technique, which is efficient and converges to second order. The approach is covered in full in Cebeci and Bradshaw[15] and Keller[16].

The coupled nonlinear system (11)–(12) is numerically integrated over the boundary layer region using an implicit finite difference technique. We use the multi-step system (11)–(12) Keller-box solution technique. The system needs to be converted into a system of first-order equations before adding any additional unknown functions. The central finite-difference method is used to discretize this first-order system, resulting in a nonlinear set of algebraic equations. We use Newton's linearization method to make them linear. It is necessary to employ the linear system of equations' matrix-vector representation.

$$AD = R \tag{14}$$

where

$$A = \begin{bmatrix} [A_1] & [C_1] & 0 & \dots & \dots \\ & [A_2] & [C_2] & 0 & \dots \\ 0 & \dots & \dots & \dots & \dots \\ 0 & \dots & [B_{j-1}] & [A_{j-1}] & [C_{j-1}] \\ 0 & \dots & \dots & [B_j] & [A_j] \end{bmatrix}$$

where that A block tridiagonal structure, where each element is a sub-matrix of order six, and N denotes the total number of grid points in the η- direction, i.e. $N = \frac{\eta_\infty - 0}{\eta_i}$ direction, i.e., with is some large numerical constant at which and are satisfied. There are also column matrices of unknown entries (D) and known entries (R). As a result, the exact values of depend on the grid size η_i and are unknown in advance. Nonetheless, is selected in the majority of our simulations such that the value solely depends on value. Enough effort is made to ensure that the final convergent solutions have the same difference between two successive values. The LU decomposition method can be used D to solve the tridiagonal structure (14) mentioned above. until the convergence-achieving solution is reached inside

We apply the far-field boundary conditions for the pseudo-similarity variable η at a finite value that is sufficient to achieve the far-field boundary conditions asymptotically for all values of the pertinent parameters considered because the computational domain in this problem must be finite but the physical domain in this problem is unbounded. Our code employs a changeable grid size and a number of flow domains to get the precise wall stress values $f''(0)$ and $g''(0)$. The Navier-Stokes equations $f'(\eta)$ and $g'(\eta)$ have boundary layer limit solutions that are velocity profiles in each case. By employing a very fine grid in the flow domain to capture any discernible flow irregularities, this Keller-box solver performs wonderfully and is flexible. Each of our simulations had an error tolerance of 10^{-7}. The velocity profiles $f'(\eta)$ and $g'(\eta)$ for various values of α and β are shown in the following figures. As soon as the Keller-box algorithm converges and the velocity profiles are generated, we determine the displacement thicknesses.

$$\delta_x = \int_0^\infty (1 - f'(\eta))d\eta, \qquad \delta_y = \int_0^\infty (1 - g'(\eta))d\eta \tag{15}$$

for various physical parameters. These results are discussed in Figure 6.

4.0 Result and Conclusion

This article discusses the physical explanations for how the intriguing parameters that enter the problem behave. Using the Keller-box approach, which is covered in the preceding part, the system (11)-(12) has been numerically solved. The shear-to-strain rate (α) and pressure gradient (β) are two of the parameters that have been numerically calculated to determine the conditions under which a

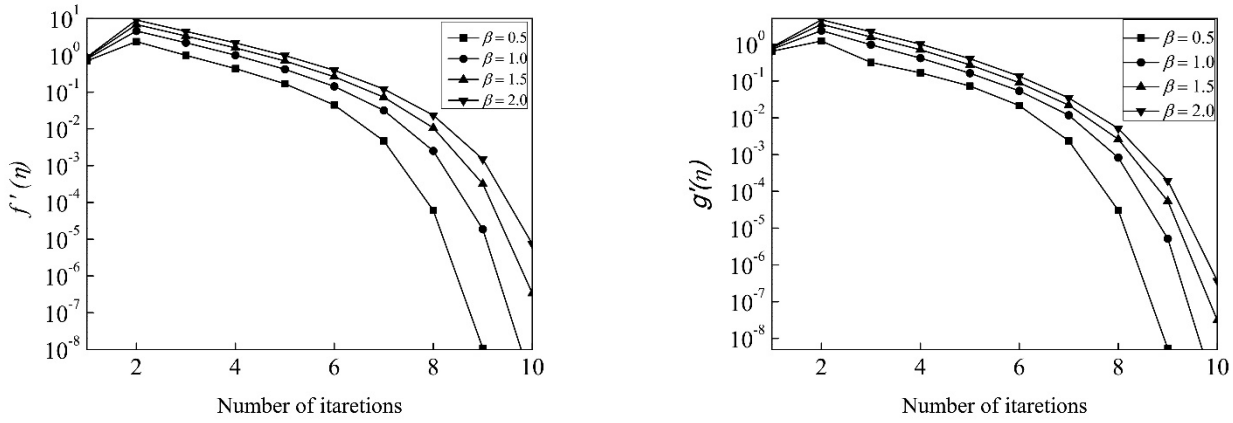

Figure 1. Variations of residual error for $f'(\eta)$ and $g'(\eta)$ for $\eta = 1$ with number of iterations.

steady flow is achievable. Finding the velocity profiles $f'(\eta)$ and $g'(\eta)$ as well as the wall shear stresses $f''(0)$ and $g''(0)$ when the Keller-box code converges to 10^{-7} is the main goal of the analysis. The residual error is used to evaluate the Keller-box method's convergence criteria. In order to do this, we have selected the continuous decay of $f'(\eta)$ and $g'(\eta)$ at η=1 as well as $f''(0)$ and $g''(0)$ as a function of the rising iteration number. Figures 1 and 2 show this for a few physical parameters (defined). Although the solutions to a linear algebraic system of equations are certain to contain errors (Biberdorf and Popova[17]), these errors can be reduced to the desired level of accuracy by choosing a better initial condition as the number of iterations increases. The figures effectively explore these. The residual error between two successive iterations reduces gradually during the first few iterations, but beyond a certain number of iterations, the error decreases in the exponential form, indicating that the solutions are converging. The results of $f''(0)$ and $g''(0)$ further support these errors, and it is important to note that they show the same general patterns. The numerical findings are shown graphically to highlight the key aspects of the model.

For $\beta = 1$ and α in (-1,1), the results of (11)-(12) have been determined using the Keller-box approach and are shown in Table 1. The acquired results are compared to those of Davey[6] and Rosenhead[1] in order to validate the newly altered equations. There is good agreement between our results and the two solutions in the table for the skin frictions $f''(0)$ and g"(0). It demonstrates that the new equation form suggested in this work has a good

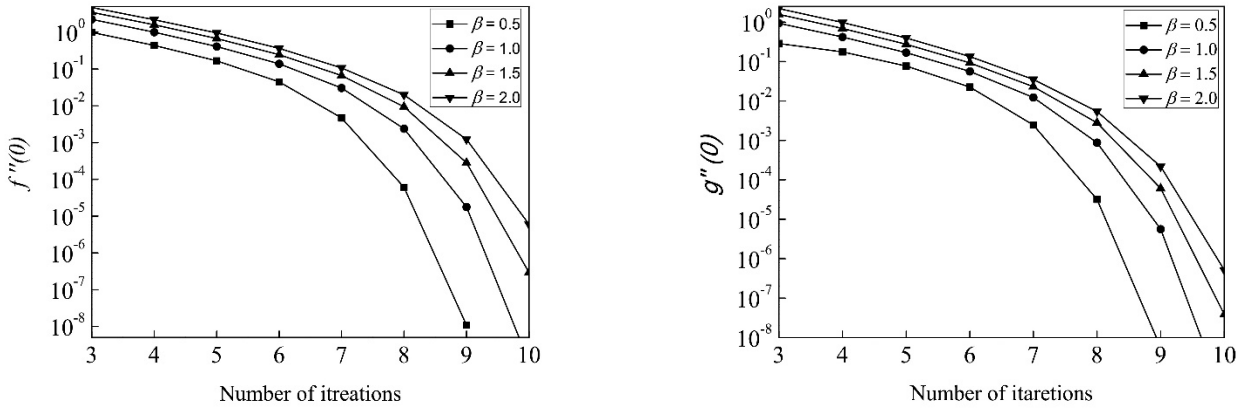

Figure 2. Variations of residual error for $f''(0)$ and $g''(0)$ with number of iterations.

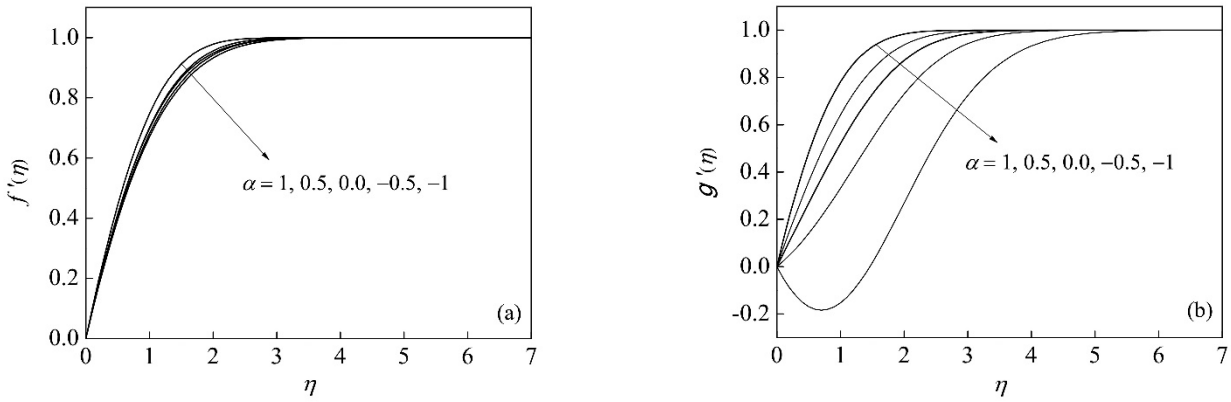

Figure 3. Variation in velocity profiles and their relationship to various values of α, keeping $\beta = 0.5$ constant.

consistency with the literature. Keep in mind that the pressure gradient forces the solution for $\alpha \in (-\infty,\infty)$ to exist. These calculations assume that η_∞ is 4, or N=401 grid points. Consecutive iterations reduce error gradually, but after a given number of iterations, error drops in the exponential form, indicating convergence of the solutions. The results of $f''(0)$ and $g''(0)$, which show that the same general tendencies are present, further support these errors. The numerical findings are graphically displayed to highlight the key characteristics of the model.

The range of parameters that emerged as the most intriguing after examining the behaviour of the physical profiles as a function of coordinate distance. The velocity profiles $f'(\eta)$ and $g'(\eta)$ are shown in Figure 3 as functions of *eta* for a pressure gradient of $\beta = 0.5$ and for various shear-to-strain rates of α. All velocity profiles $f'(\eta)$ and $g'(\eta)$ meet their derivative condition at infinity (i.e., $f'(\eta) \to 1$, $g'(\eta) \to 1$ as, $\eta \to \infty$,). This is obvious. Remember that the derivative requirement is satisfied at the value of *N*, which is 701 ($\eta_\infty : 7$). Ten iterations are required for convergence. In contrast to Figure 3a, picture 3b shows how the velocity curve behaves differently for various values of $\alpha = 0$. For $\alpha = 0$, the flow shows a propensity toward boundary-layer separation; for example, look at the curve for α = -0.5; nevertheless, for α = -1, the flow totally separates at the wedge surface, where the boundary-layer assumptions end, and then quickly reattaches for some η. Additionally, for other values of α = 0.0,0.5,1, , the profiles approach the wedge surface, resulting in a thin boundary layer. Figure 3a, on the other hand, makes it abundantly evident that all of the curves are harmless. It suggests that when the velocity profiles become more localised at the surface, the thickness of the boundary layer is reduced.

Figure 4 depicts the impact of a favourable pressure gradient *beta* on the velocity $f'(\eta)$ and $g'(\eta)$ in two directions at various shear-to-strain rate parameters (α). The velocity curves are seen to monotonically tend toward their asymptotic terminal state. Additionally, velocity profiles drop off as pressure gradient β increases. Additionally, as the pressure gradient rises, the thickness of the momentum boundary-layer diminishes. The velocity curves are clearly within the bounds in all of the figures. It should be noted that in the three-dimensional boundary layers, there is no reverse flow for favourable pressure gradient. The profiles become more stable under the favourable pressure gradient, which naturally keeps them from separating. Calculations with a rising pressure gradient showed unmistakably that the profiles were constrained to an area near the wedge surface.

When the Keller-box code converges and the velocity profiles are created, the key findings in terms of wall shear stresses are now discussed. Figure 5 explores these wall shear stresses as a function of the shear-to-strain rate parameter α in the range $\alpha \in [-5,5]$ (which can be expanded to (-∞,∞)). The figure shows the values $f''(0)$ and $g''(0)$ derived from the Keller-box code as dashed and solid lines, respectively. It should be noticed that all tested $g''(0)$ values gradually increase as α is raised

from -5 to 5. Unexpectedly, *g″(0)* curves change their orientations at $\alpha = 0$, as is shown in the illustration. The values for rising α values gradually increase for *f″(0)*, in contrast. The curves for *f″(0)* become nearly flat and growth becomes constant beyond a certain α(:10).

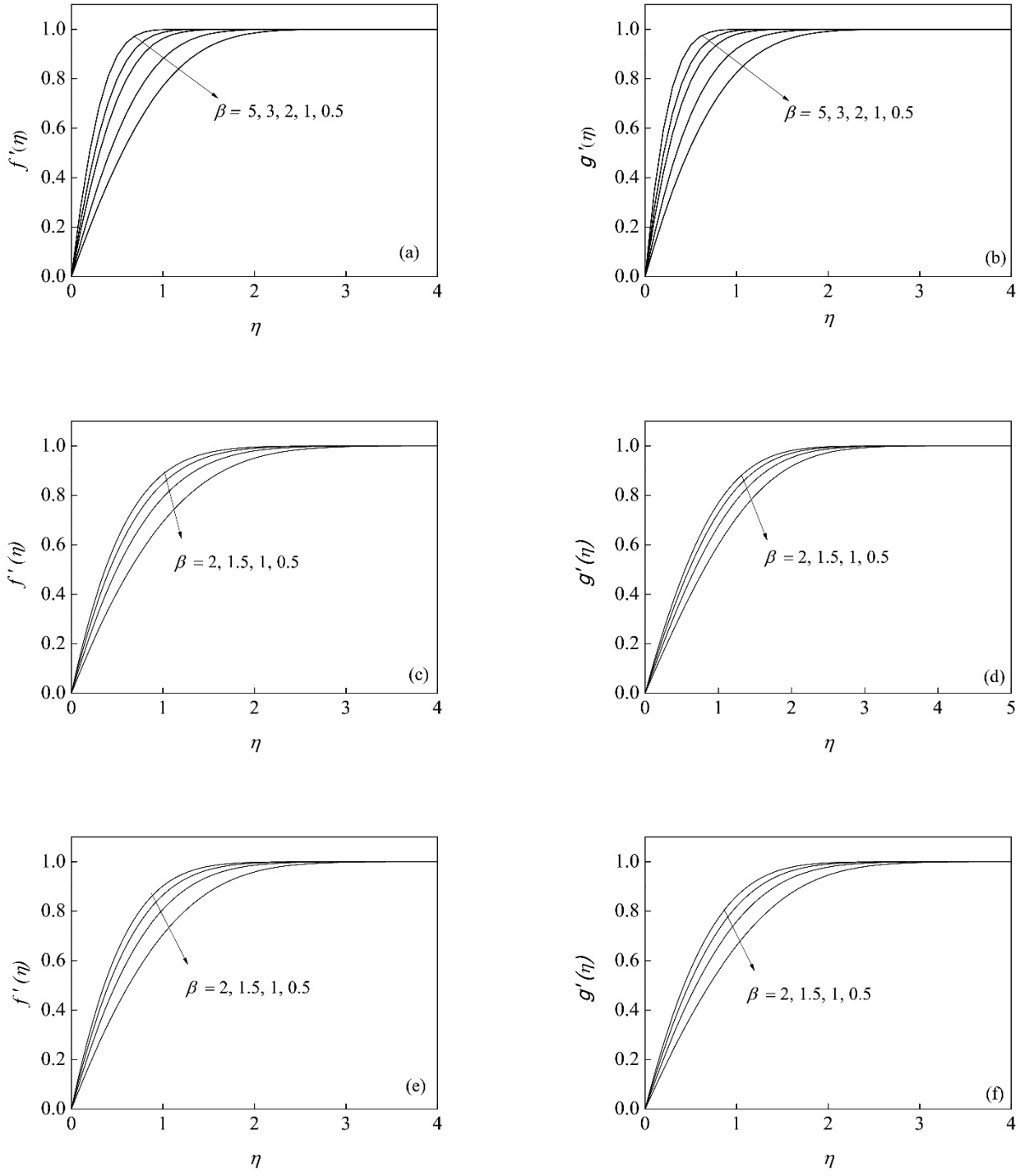

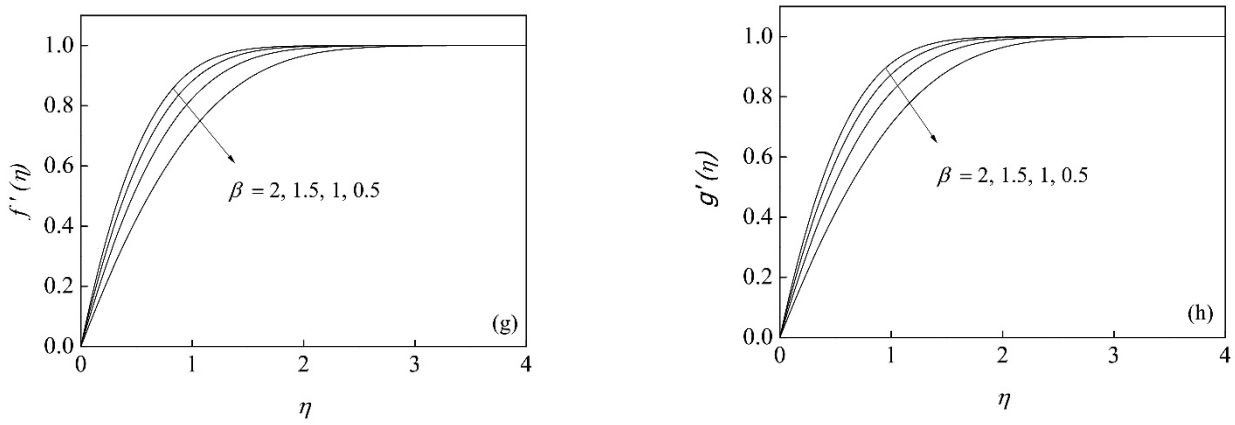

Figure 4. Variation in velocity profiles and their relationship to various values of β, for i. (a) and (b) for $\alpha = 2.0$, ii. (c) and (d) for $\alpha = 0.3$ iii. (e) and (d) for $\alpha = 0.6$, iv. (g) and (h) for $\alpha = 0.9$.

Table 1. The numerically solutions of skin frictions *f″(0)* and *g″(0)* (Compared with literature results)

β = 1						
α	**f″(0) (Present)**	**f″(0) (Davey)**	**f″(0) (Rosenhead)**	**g″(0) (Present)**	**g″(0) (Davey)**	**g″(0) (Rosenhead)**
-1	1.27339892	1.2729	—	-0.80261050	-0.8112	—
-0.75	1.24840014	1.2473	—	-0.48302587	-0.4821	—
-0.5	1.23112719	1.2302	—	-0.11188326	-0.1115	—
-0.25	1.22603177	1.2251	—	0.26800659	0.2680	—
0	1.23357914	1.2326	1.233	0.57085080	0.5705	0.570
0.25	1.24875909	—	1.247	0.80582232	—	0.805
0.5	1.26820644	—	1.267	0.99912778	—	0.998
0.75	1.29018795	—	1.288	1.16570303	—	1.64
1	1.31373362	—	1.312	1.31373362	—	1.312

Figure 6 also shows the displacement thicknesses as functions of alpha for various beta. Here, dashed and solid lines stand in for δ_y and δ_x, respectively. The Simpson's ⅓rd rule is used to do integration on the data acquired from (15). The Keller-box technique uses this piece of code. While there is a slight discrepancy between the δ_y and δ_x, values in this example, the curves for both δ_x and δ_y become flat as α increases. This implies that for every set of parameters, the velocity profiles are linked to the wedge surface and the boundary-layer thicknesses drop. As a result, the flow in the boundary-layer is constantly convected along the direction of the wedge's wall. For all values of the accelerated pressure gradient parameter β, this is shown.

We noted in the literature that the analysis of three-dimensional boundary layers is only possible for $\beta = 1$ (i.e., the point at which $\alpha \in [-1,1]$ stagnates). Here, we've broadened the solutions' applicability to various beta values. We compared our numerical solution to the Davey[6] equation to confirm the equation. However,

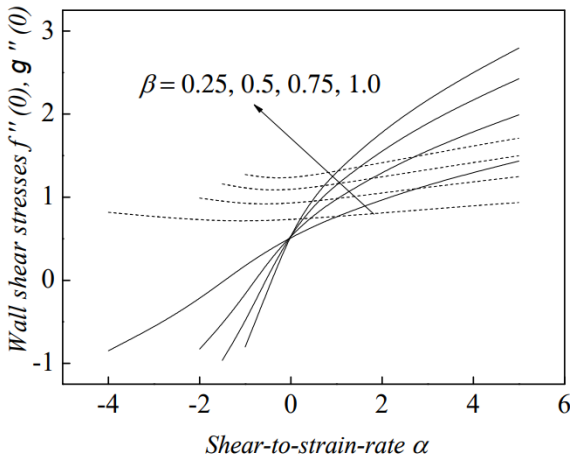

Figure 5. The variation of the skin fricition in both directions as a function of α for different β.

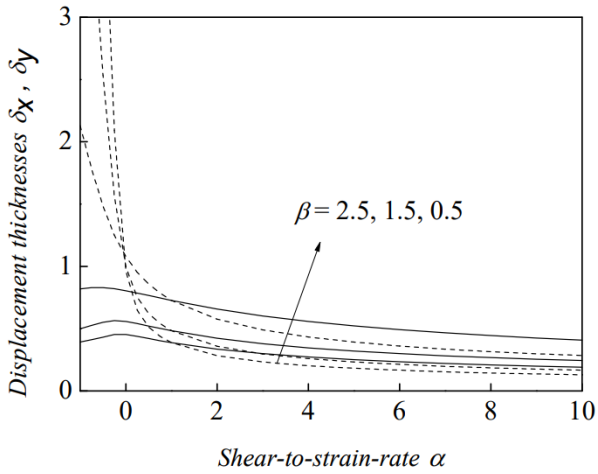

Figure 6. The variation of the displacement thicknesses in both directions as a function of α for different β.

the negative pressure gradient (β = 0) has no known solutions. For an unfavourable pressure gradient, we tried several initial circumstances and grid lengths, but there isn't a solution. The causes for the lack of solutions for negative β are thus a further significant question, and we anticipate that the addition of the magnetic field in three-dimensional will aid us in this instance, which is a future subject of interest.

5.0 Acknowledgments

Author thankful to the reviewers for valuable comments which improve the quality of article, and also Organizers of ICARES-2022, RIT.

6.0 References

1. Van Dyke M. Laminar Boundary Layers. Edited by L. ROSENHEAD. Oxford University Press, 1963. 688pp. aE4. 10s. Journal of Fluid Mechanics. 1964 Mar; 18(3):477-80.
2. Howarth L. XXV. The boundary layer in three dimensional flow. Part I. Derivation of the equations for flow along a general curved surface. The London, Edinburgh, and Dublin Philosophical Magazine and Journal of Science. 1951 Mar 1; 42(326):239-43.
3. Howarth L. CXLIV. The boundary layer in three dimensional flow. —Part II. The flow near a stagnation point. The London, Edinburgh, and Dublin Philosophical Magazine and Journal of Science. 1951 Dec 1; 42(335):1433-40.
4. Weidman PD. Non-axisymmetric Homann stagnation-point flows. Journal of Fluid Mechanics. 2012 Jul; 702:460-9.
5. Howarth L. CXXIX. Note on the boundary layer on a rotating sphere. The London, Edinburgh, and Dublin Philosophical Magazine and Journal of Science. 1951 Nov 1; 42(334):1308-15.
6. Davey A. Boundary-layer flow at a saddle point of attachment. Journal of Fluid Mechanics. 1961 Jun; 10(4):593-610.
7. Libby PA. Heat and mass transfer at a general three-dimensional stagnation point. AIAA Journal. 1967 Mar; 5(3):507-17.
8. Davey A, Schofield D. Three-dimensional flow near a two-dimensional stagnation point. Journal of Fluid Mechanics. 1967 Apr; 28(1):149-51.
9. Wang CY. The three-dimensional flow due to a stretching flat surface. The physics of fluids. 1984 Aug; 27(8):1915-7.
10. Devi CS, Takhar HS, Nath G. Unsteady, three-dimensional, boundary-layer flow due to a stretching surface. International Journal of Heat and Mass Transfer. 1986 Dec 1; 29(12):1996-9.
11. Hewitt RE, Duck PW, Stow SR. Continua of states in boundary-layer flows. Journal of Fluid Mechanics. 2002 Oct; 468:121-52.
12. Schlichting H, Gersten K. Boundary-layer theory. Springer; 2016 Oct 4.

13. Benzi R, Ching ES, Chu VW. Heat transport by laminar boundary layer flow with polymers. Journal of fluid mechanics. 2012 Apr; 696:330-44.
14. Benzi R, Ching ES, Wilson CK, Wang Y. Heat transport modification by finitely extensible polymers in laminar boundary layer flow. Journal of Fluid Mechanics. 2016 Feb; 788:337-57.
15. Cebeci T, Bradshaw P. Momentum transfer in boundary layers. Washington. 1977.
16. Keller HB. Numerical methods in boundary-layer theory. Annual Review of Fluid Mechanics. 1978 Jan; 10(1):417-33.
17. Biberdrof, EA, Popova NI. Guaranteed accuracy of current methods in linear algebra. Novosibirsk, Izd-vo So RAN, 2006, 320p.